1

Introduction for Biomimetic Superhydrophobic Materials

Wetting phenomena are found abundantly in our body, our surroundings, and our daily lives. Our eyes repel condensed water for a clear vision, and the articular cartilage is superwetting to achieve ultralow wear. When it is raining, we can glance the raindrop rolling down from some kinds of plant leaves while still leaving a trail of water trace on other kinds of plant leaves. Wetting behavior is also closely related to laundry, froth flotation, printing and dyeing, oil extraction, welding materials, lubricating systems, and so on.

Wettability is determined by the interaction of a surface and interface between a solid and a liquid. The interface is a transition region forming a boundary between two different phases of matter. Exactly speaking, a solid (liquid) surface means the interface between a solid (liquid) and vacuum or a gas. If the liquid is water, the wetting behavior falls into several categories, namely superhydrophilicity, hydrophilicity, hydrophobicity, and superhydrophobicity. As our book will show in detail in the following part, superhydrophobicity is usually defined as the contact angle (CA) of a water drop on a solid surface >150° and a sliding angle (SA) <10°. It is also possible to change a solid surface from hydrophilic (or hydrophobic) to superhydrophobic.

Tuning the wettability of a liquid drop on solid surfaces is an important issue attracting more and more interest from both fundamental and practical perspectives. The answers to such question do help us find the miracle and power of the biomimetic ideology.

Biomimetic materials mean mimicking organisms with the aim of designing artificial materials with desirable functions [1]. In Nature, there are many perfect functional materials with various structures, and the needs of adaptation and survival are indeed the result of esthetic functional systems. Geckos are known for their excellent ability to run on ceilings, and studying their feet would inspire technologists to design of a variety of dry adhesives [1, 2]. The water strider has a remarkable ability to stand, walk on, and even leap from a water surface effortlessly [3]. This skill derives from the superior water repellency of its legs, which possess thousands of tiny setae with fine nano-grooved structures. Investigating the water strider's leg would be helpful in developing some water-standing/walking microdevices employed in monitoring the activities on a water surface [4]. The lotus leaf with nanoscale details superimposed on a microscale structure is a typical example and has an impressive self-cleaning feature. This leaf surface is endowed with a large contact angle >160° and a sliding angle <3°, and this results in the well-known

Surfaces and Interfaces of Biomimetic Superhydrophobic Materials, First Edition.
Zhiguang Guo and Fuchao Yang.

"*lotus effect*" [5a]. Barthlott suggested that this property primarily originates from the cooperative effect of micrometer-scale papillae on the rough surfaces and hydrophobic epicuticular wax [5b]. This was a very interesting and important discovery. Learning from Nature, tremendous progress in biomimetic superhydrophobic architecture engineering has been achieved using a range of methods. The advantages, disadvantages, and typical examples of each main method will be introduced in this book.

In this chapter, the fabrication methods of certain superhydrophobic materials will be mentioned succinctly, and the amazing applications of biomimetic superhydrophobic materials are explored and elaborately introduced. It is a fact that a full-scale introduction of the applications of biomimetic superhydrophobic materials is beyond us. So the adhesive behavior and oil/water separation properties of superhydrophobic materials, discussed in other chapters, are not intended to be presented repeatedly. The main relative aspects we focus on in this part will cover novel fields such as water harvesting, self-cleaning, corrosion resistance, photochromic superhydrophobicity, robust superhydrophobicity, conductive and transparent superhydrophobicity, anti-fingerprint superhydrophobicity, and the anti-icing ability of superhydrophobicity. We hope this arrangement can help arouse the readers' interest and encourage the reading of other chapters.

1.1 Water Harvesting

An alternating pattern of superhydrophobic and hydrophilic hybrid materials has an important applied background. The available freshwater resources for humans in the poor and rural areas are extremely scarce. In recent years, learning from Nature has motivated extensive interest in the field of bioinspired superwettable materials [6], which show a huge potential to effectively address this very serious issue. Namib Desert beetles feature an interesting fog-harvesting property resulting from the alternating waxy hydrophobic and nonwaxy hydrophilic regions on their dorsal body [7]. Spider silk can collect fog from the atmosphere due to its periodic spindle-knots with a combined structure and chemical gradient [8]. These typical examples from Nature offer the inspiration to synthesize corresponding biomimetic water-collecting materials. Some representative works from our group and other laboratories are described in the following.

Because of their high surface energy, metal nanoparticles (NPs) are known to be *extremely hydrophilic substances*. Hydrophobic properties of the metal NPs can be obtained if these particles are pretreated with low-surface-energy chemicals. *n*-Octadecyl thiol, which possesses low surface energy, was selected as the modifier to obtain a superhydrophobic–superhydrophilic hybrid fabric depending on the thiol's selective modification of NPs on the fabric. Based on this, two adjacent transition metals, Fe and Co, were selected and coated on a commercially available fabric via a facile *in situ* growth method [9]. The surface of Co NPs could be modified by *n*-octadecyl thiol and transformed into hydrophobic NPs. However, the Fe NPs could not be modified by *n*-octadecyl thiol under our

experimental conditions. Thus, they retained the hydrophilic property. The as-prepared fabric with these two kinds of NPs evenly distributed on the surface is termed a *superhydrophobic–superhydrophilic hybrid fabric* because it shows superhydrophobicity and possesses many superhydrophilic spots. These two kinds of NPs were evenly distributed on the fabrics, and their coating amounts were easily controlled by altering the concentrations and the proportion of the two kinds of ions in the precursor solution. Because of the selective modification, the wettability of the fabrics is linearly dependent of their concentration ratio and varies over a wide range from superhydrophilic to superhydrophobic. To obtain a superior water-harvesting fabric, the concentration ratio must be appropriate because values that are either too small (Fe NPs are dominant) or too large (Co NPs are dominant) are not beneficial for water harvesting. This kind of material might help in solving the global shortage of fresh water via an energy-saving strategy. This material has been found successful in realizing water harvesting similar to the desert beetle that collects micro droplets of water from the morning fog.

Inspired by Nature and beyond it, Peng *et al.* fabricated a new kind of material that could achieve fog harvesting even under windless conditions [10]. They dispersed 200 mg Co MPs in the microscale with an average diameter of 2 mm into each mechanical hole of the array. Poly(dimethylsiloxane) (PDMS) pre-polymer containing 0.1 equiv. of curing agents was cast on the template filled with cobalt magnetic particle (Co MPs) with the help of a vacuum pump. Here, mechanical perforation and template replica technology were also applied, whereby Co MPs were added in the latter step. Meanwhile, a magnet of 60 mm diameter and 50 mm thickness was prepared. The sample was placed on the top of a permanent magnet with a superficial magnetic field intensity of about 0.9 T during the process of degassing and curing so as to make the Co MPs vertically aligned in the holes. As shown in Figure 1.1a, the conical array responded to the magnetic field. Using a high-speed (charge-coupled device) CCD camera, the movements of cone arrays responding to the magnetic field were recorded (Figure 1.1b,c). When the magnet was placed directly over the sample, the cactus-spine-like cones were totally upright. The cone arrays could collect fog in a spontaneous and continuous way if a moving magnetic field was provided (Figure 1.1d). However, no water drop deposited on the arrays without the magnetic field (Figure 1.1e). By integrating cactus-inspired spine structures with magnetically responsive flexible conical arrays, magnetically induced fog harvesting under windless conditions was achieved. To meet the urgent demand for the basic water requirement, a much larger scale of the as-prepared, magnetically induced fog collector should be fabricated. In windless and foggy regions, the magnetically induced fog harvesting system has great advantages and promising applications. Furthermore, it may serve in our daily lives as an effective method for further optimization of oil mist purification and fog harvesting strategies.

Using the fluid coating method, Jiang and coworkers developed bioinspired fibers with periodic spindle-knots on a large scale [11]. The nylon fibers in the polymer solution reservoir were fabricated by capillary tubes (about 400 μm inner diameter), which were composed of poly(methyl methacrylate) (PMMA) dissolved in *N*,*N*-dimethylformamide (DMF) with a weight percentage of 11%, and

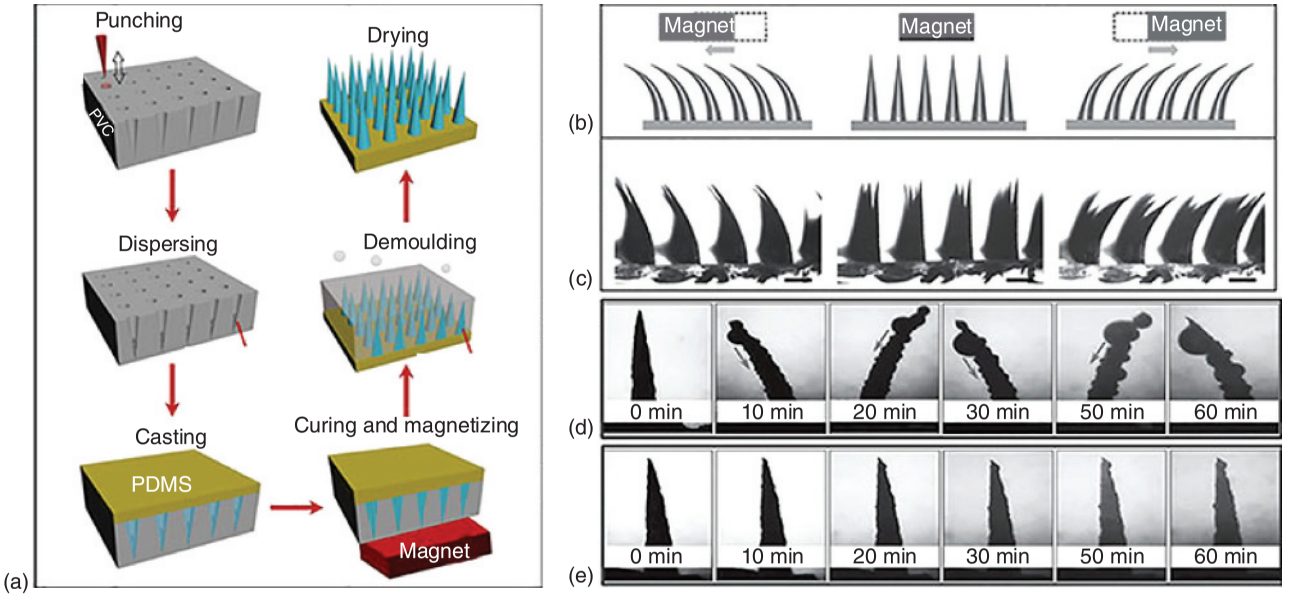

Figure 1.1 (a) Schematic of the fabrication of cactus-inspired conical arrays and (b) the magnetically induced conical array responses. (c) Charge-coupled device (CCD) camera observations in response to a magnet. Scale bar: 1 mm. (d) Magnetically driven cone and (e) a static cone placed in the same fog chamber at different time periods. (Peng *et al*. 2015 [10]. Reproduced with permission of John Wiley and Sons.)

the end of the fiber was connected to a motor. At the same time, the solution container was controlled to be 2 cm × 3.5 cm × 3 cm (width × length × height) in size. As it moved out of the reservoir, the polymer solution was coated on the fiber. The cylindrical polymer film was broken up into droplets because of the Rayleigh instability, and periodic spindle-knots on the fiber were obtained after solvent evaporation. In Figure 1.2a, when the concentration of PMMA/DMF solution increased, the critical velocity ($V_{critical}$) decreased. The spindle-knots on the fiber could be formed only if the drawing velocity was more than $V_{critical}$. In Figure 1.2b, the spindle-knot attained the largest size at a velocity of 1.44 mm s^{-1} (13% by weight PMMA/DMF solution). The solution parameters and fiber-drawing velocities were proved to play very important roles in the formation of the spindle-knots. As shown in Figure 1.2c–g, the bioinspired fiber was endowed with directional water-collecting ability. Inspired by the beautiful sight of a spider's web decorated with shiny water droplets, novel and functional fiber materials were designed and fabricated that were endowed with water collection abilities.

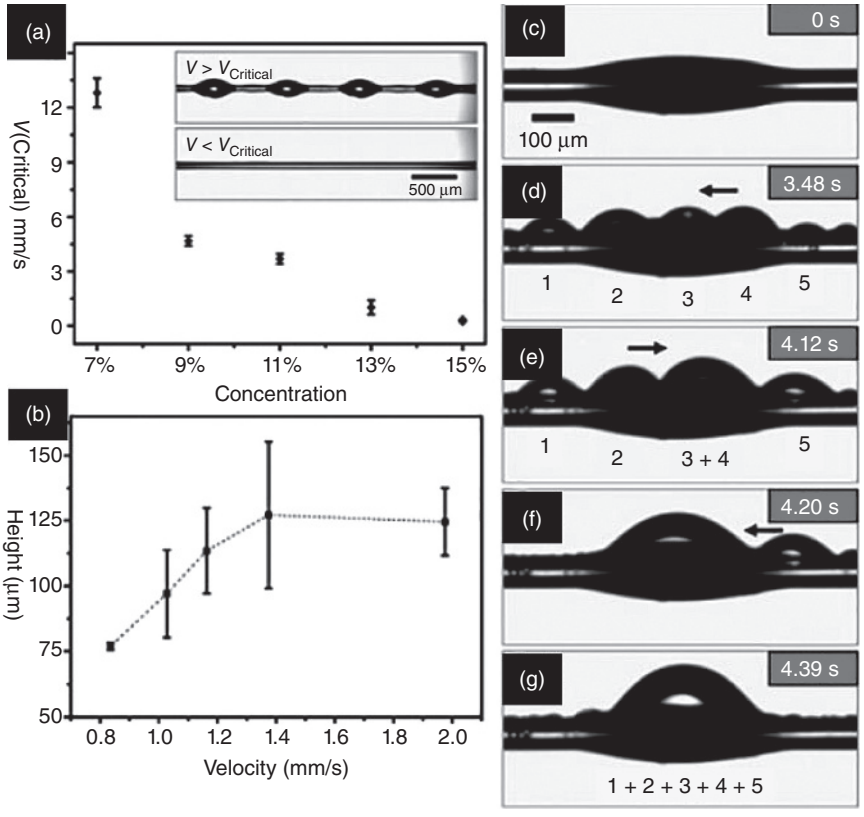

Figure 1.2 (a) Relationship between the critical velocity ($V_{critical}$) and the concentration of the PMMA/DMF solution. The spindle-knots could be constructed when $V > V_{critical}$, or vice versa. (b) Size of the spindle-knots as a function of the drawing velocity. (c–g) Directional water-collection process on a bioinspired fiber with a PMMA spindle-knot. (Bai *et al*. 2016 [11]. Reproduced with John Wiley and Sons.)

Also, TiO_2 has been used in a water collection system. It is well known that TiO_2 manifests switching wettabilities under UV light irradiation, attributable to its excellent photocatalytic property [12]. By integrating the water-collecting mechanisms of both desert beetles and spider silk, Zheng *et al.* successfully designed and fabricated TiO_2-based materials with star-shaped wettability patterns [8a]. In our study, TiO_2 was also introduced in fabricating water-collecting materials, which mainly utilized the alternative modifications between Cu, TiO_2, and thiols [13]. Cu can easily be modified by thiols and can act as the hydrophobic areas, while TiO_2 cannot be modified by thiols and serves as hydrophilic sites. The hybrid engineered surfaces therefore inspired their synthesis. At a precursor molar rate (Cu:TiO_2) of 9 : 1, the as-prepared sample, with a water contact angle (WCA) and rolling angle (RA) of 155.1° and 4.5°, respectively, exhibited the highest water collection rate (WCR) of 1309.9 mg/h/cm^2. The fabrication of superhydrophobic hybrid materials may show new directions for future fog collection projects and be indicative for mass production, demonstrating promising applications to solve the growing global water shortage. In another study [14], we synthesized successfully a superhydrophilic sample with two embedded superhydrophobic circles, and the fabrication process could be accomplished by a simple and quick route at room temperature. Importantly, this material showed high efficiency for fog capture with a WCR of 1316.9 mg/h/cm^2, which is an advantage over uniformly superhydrophobic and superhydrophilic samples. It is worth mentioning that the water collection of these samples could be repeated over 10 times without obvious variations in the WCR.

Functional surfaces with superior water collection, as promising materials, are required for the abatement of water shortage. Though a number of water-collecting materials have been fabricated, there are still some problems that need to be solved. Also, the gap between basic research and applied technology should be bridged, which is of great importance in realizing the transformation between experimental results and industrial achievements. It is believed that water-collecting materials will pave the way for functional practical applications to solve the current severe water shortage in dry and less economically developed areas of the earth.

1.2 Self-Cleaning

No dust can reside on a lotus leaf after rain because of its effective water repellency. Bearing this in mind, we tried to biomimetically construct artificial superhydrophobic materials to study their self-cleaning effect. We have fabricated a kind of transparent liquid that can form transparent superhydrophobic films on various substrates by spraying [15]. The results showed that the spray exhibits excellent self-cleaning properties, which are very vital for their promising applications in industry. To evaluate the effect of antifouling, Figure 1.3a shows muddy water poured on a white fabric with a superhydrophobic coating. Figure 1.3b shows that the coated fabric was well kept and had no muddy water trail on the surface, while the uncoated fabric on the left had much muddy water on it. The coated fabric exhibits surface properties like the lotus leaf, which lies in silt but is

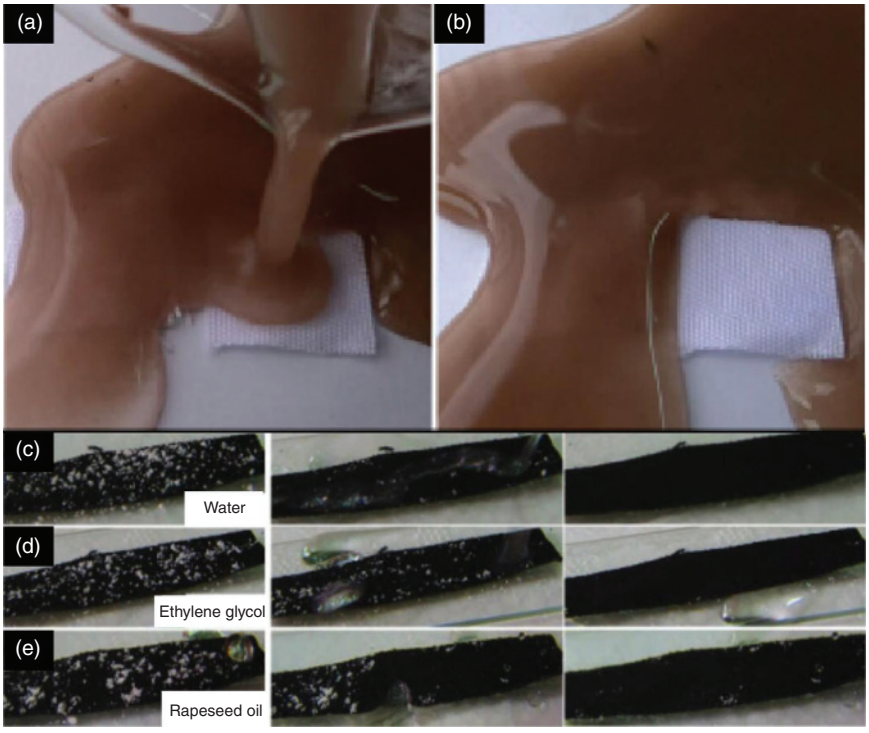

Figure 1.3 (a, b) Digital photographs of a coated white fabric used in antifouling (Dong *et al*. 2015 [15]. Reproduced with permission of The Chemical Society of Japan). (c) Description of the self-cleaning ability of strong amphiphobic fabric through the removal of chalk dust from the surface by the movement of water, ethylene glycol, and rapeseed oil. (Zeng *et al*. 2014 [16]. Reproduced with permission of The Chemical Society of Japan.)

not imbrued. We have also developed a facile, low-cost fabrication strategy for strong amphiphobic coating [16]. The detailed procedure included the construction of a CuO hierarchical structure on porous substrates (nickel foam and fabric) and the subsequent modification with perfluorodecanethiol. The CuO-coated nickel foam and fabric showed excellent repellency to water and oils at the same time. Water and oil droplets on their surface can easily roll off from the surface. Furthermore, these samples exhibited strong oleophobicity for different types of oils such as ethylene glycol, rapeseed oil, hexadecane, glycerol, and decane. It is worth mentioning that the surface of as-prepared samples showed excellent oil-self-cleaning properties, which would extend its potential applications in some oily surroundings. Self-cleaning effect of a surface with liquid repellency plays an important role in many practical applications. In order to investigate the self-cleaning behavior, chalk powder was employed as contaminant that was dusted on the surface of a lotus leaf and CuO-coated fabric (Figure 1.3c–e). For the CuO-coated fabric with superhydrophobicity and strong oleophobicity, the liquid droplets could take away the chalk dust on the surface when sliding on the surface, as shown in Figure 1.3c–e. Importantly, ethylene glycol and rapeseed oil were observed to easily move from the contaminated surface and take the chalk

dust away effortlessly, suggesting that the CuO-coated fabrics possessed good self-cleaning property against both water and oil, which is attributed to the high contact angle and low sliding angle of the constructed surface.

Photoinduced self-cleaning is another kind of smart self-cleaning property. In our work [17], TiO_2 coatings with hierarchical rutile TiO_2 flowers on fluorine-doped tin oxide substrate were fabricated through a simple one-step hydrothermal method. The flower-like coatings exhibited superhydrophilicity in air and superoleophobicity under water with a contact angle of 157° (Figure 1.4a, left column), presenting good underwater self-cleaning performance. The as-prepared films were contaminated with an *n*-pentane solution containing oleic acid to study its photoinduced self-cleaning. Because of the high surface free energy of the TiO_2 material, the film was superhydrophilic in air and superoleophobic

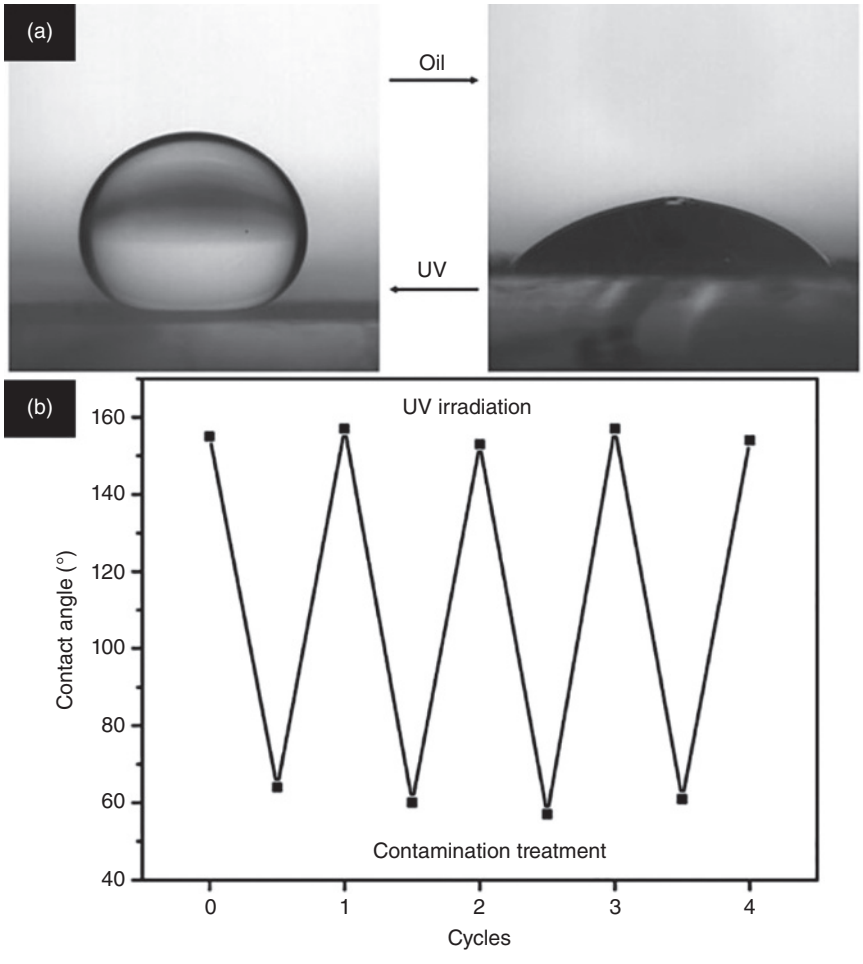

Figure 1.4 (a) Photographs of an oil droplet on the TiO_2 flower coatings after contamination treatment and UV irradiation. (b) Reversible changes of OCA on the sample during cyclic alternations of contamination treatment and UV irradiation.

under water before oil contamination. As for contamination, the sample was dipped into the above solution for 5 s and then withdrawn at a speed of 9.5 mm/s, followed by drying at 60 °C for 10 min. After the contamination treatment, the film lost its superwetting property, with the WCA increasing to 137° and the oil contact angle (OCA) decreasing to 64° (Figure 1.4a, right column). In this case, the underwater oil–solid contact can be termed as *a homogeneous wetting state*. However, the film turns hydrophobic in air and oleophilic under water if it is discretely contaminated by oleic acid spots. The surface free energy decreased after the contamination, resulting in the increase of WCA (from 0° to 137°). Because of some oleic acid spots trapped between the oil and the film, the underwater oil–solid contact in this situation is the so-called heterogeneous wetting regime. After irradiating by UV light (for 2 h), the film recovered its superamphiphilic and underwater superoleophobic properties. This shows that the TiO_2 coatings exhibit excellent self-cleaning ability under UV irradiation. Furthermore, as shown in Figure 1.4b, this process could be continuously repeated for several cycles without the loss of its responsivity, and the as-prepared self-cleaning surface had good stability.

Surfaces with self-cleaning property can remove contaminates on superhydrophobic materials, which is of great importance for water repellency. Moreover, self-cleaning is a decisive factor for applications of superhydrophobic materials.

1.3 Corrosion Resistance

Corrosion due to various active metals is of great importance in deciding the lifetime of some engineering materials. Interestingly, superhydrophobic coatings on the surfaces of metals can bring about superb corrosion resistance, which expands their scope of application and prolongs the service life of the metallic materials. On the basis of this, we have reported a simple method for preparing a two-dimensional material based on commercially available stainless steel mesh and copper mesh substrates functionalized by depositing nanoscale polypyrrole (PPy) particles, followed by modification of a low-surface-energy material such as fluoroalkylsilane (FAS) [18]. Such superhydrophobic samples are endowed with good anticorrosion properties for several metals to a greater extent. We applied several corrosive liquids, such as acidic, basic, and salt aqueous solutions, to test the corrosion resistance. Corrosive liquids on the surface of superhydrophobic PPy-coated substrates stood uniformly on the surface and maintained a spherical shape. All samples' WCAs were >150°. Utilizing polarization measurements, we also compared the anticorrosion properties of superhydrophobic PPy-coated metal meshes with those of bare metal samples. The corrosion characteristics of such samples in 3.5 wt% NaCl aqueous solution, 0.5 M H_2SO_4 solution, and 1 M NaOH solution are given in Table 1.1. According to Table 1.1, the i_{corr} values of uncoated surfaces appear to be relatively high. This is because the bare substrate surfaces are in an unstable state and copper or iron becomes ions quickly, thus promoting corrosion.

Generally, a lower corrosion current density or a higher corrosion potential corresponds to a lower corrosion rate and better corrosion resistance. From

Table 1.1, we can find that the corrosion potential and the corrosion current of the superhydrophobic PPy-coated copper meshes were 0.9716 V and 4.172×10^{-6} A, respectively, whereas the corresponding values for bare copper meshes were 0.1643 V and 7.817×10^{-5} A. The shift of the corrosion potential (by ~1.13 V) in the positive direction indicates that the superhydrophobic PPy coatings act as the effective anodic protective coating rather than offering sacrificial corrosion protection. By the deposition of superhydrophobic coating on copper mesh substrates, the corrosion current decreases by one order of magnitude, showing the significant improvement of corrosion resistance. When bare copper mesh substrates are immersed in corrosive media, the passive oxide breaks down and severe corrosion begins. Importantly, the corrosion resistance of the superhydrophobic coating was achieved by coating the bare substrates with nanoscale PPy and modifying them with a low-surface-energy material. The reason for this is that air can be easily trapped in the pits and cavities between the PPy particles, and the trapped air can serve as a first barrier layer; then the conductive polymer coating can act as the second effective barrier to the inward diffusion of Cl^-, thus inhibiting the corrosion of the substrates. In the same way, the i_{corr} of superhydrophobic stainless steel mesh samples show a decrease compared to the corresponding bare substrates while the E_{corr} increases (Table 1.1), meaning a better anticorrosion behavior of superhydrophobic samples than the bare substrates. It is believed that the double barrier layers, which consist of the trapped air layer and the PPy layer, on the substrates could guard against the outside corrosive ions, and thereby improve the corrosion resistance of such substrates to a great extent.

Aluminum alloys are important engineering materials. Feng *et al.* fabricated superhydrophobic aluminum alloy surfaces by a facile and environmentally friendly method, including boiling water treatment and polymer chain modification [19]. The corrosion resistance of the superhydrophobic Al sheet was evaluated by electrochemical experiments, and the resulting potentiodynamic polarization curves of the Al sheet samples in 3.5 wt% of NaCl solution were obtained using the Tafel extrapolation method. The corrosion resistance can be described by the corrosion current density (i_{corr}) or the corrosion potential (E_{corr}). The obtained superhydrophobic aluminum alloys, with a CA of 153.6°, showed excellent corrosion resistance, as shown in Figure 1.5. In detail, the E_{corr} and i_{corr} of the cleaned Al sheet were −1.35 V and 1.74×10^{-4} A/cm^2, respectively. By contrast, the E_{corr} and i_{corr} of a polystyrene (PS)-modified Al sheet increased to −0.95 V and decreased to 1.16×10^{-5} A/cm^2. The corrosion potential of the superhydrophobic Al sheet is more positive, while the corrosion current density is much lower than that of the cleaned Al sheet. The increase of E_{corr} in the positive direction and the decrease of i_{corr} can be linked to the protective function of the superhydrophobic film formed on the Al surfaces. Why does the superhydrophobic Al sheet show excellent corrosion resistance? This phenomenon can be explained by the fact that the superhydrophobic surface can repel any hydrophilic molecules or ions coming into contact with it. That is to say, the corrosive ions (Cl^- in NaCl solution) cannot migrate and penetrate the Al surface. So the corrosion resistance of the Al sheet is improved greatly by its acquired superhydrophobic property.

Table 1.1 Corrosion characteristics on the surfaces of bare copper mesh, superhydrophobic PPy-coated copper mesh, bare stainless steel mesh, superhydrophobic PPy-coated stainless steel mesh.

	Corrosion characteristics					
	3.5 wt% NaCl solution		0.5 M H_2SO_4 solution		1 M NaOH solution	
Samples	i_{corr} (A)	E_{corr} (V)	i_{corr} (A)	E_{corr} (V)	i_{corr} (A)	E_{corr} (V)
Bare copper mesh	7.817×10^{-5}	0.1643	1.017×10^{-4}	−0.2352	8.913×10^{-4}	−0.5863
Superhydrophobic copper mesh	4.172×10^{-6}	0.9716	7.160×10^{-6}	−0.0575	5.796×10^{-4}	−0.3357
Bare stainless steel mesh	6.821×10^{-5}	−0.3037	2.400×10^{-4}	−0.1974	5.702×10^{-5}	−0.3092
Superhydroophobic stainless steel mesh	2.224×10^{-5}	0.1224	3.726×10^{-5}	0.1444	1.067×10^{-5}	−0.2106

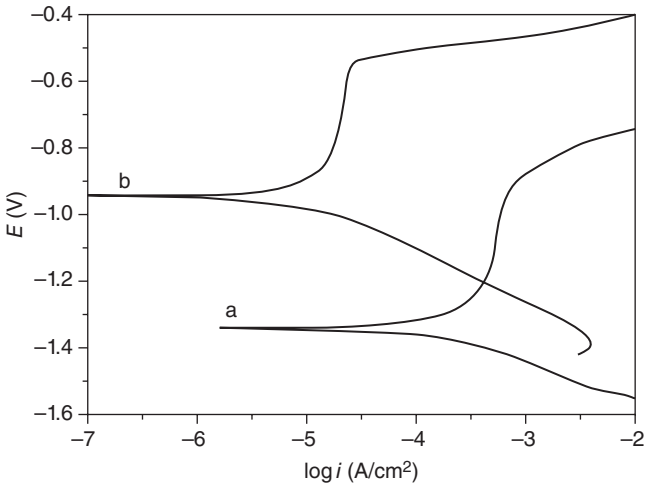

Figure 1.5 Polarization curves of the Al sheet: (a) clean and (b) PS-modified. (Feng *et al*. 2015 [19]. Reproduced with permission of John Wiley and Sons.)

Also for the corrosion protection, Xu *et al.* reported a simple approach for the preparation of superhydrophobic polyaniline (PANI) [20]. In their work, PANI was synthesized by oxidative polymerization of aniline with ammonium persulfate (APS). Subsequently, PANI was modified by different surfactants (sodium dodecylbenzenesulfonate, poly(ethylene glycol), and cetyltrimethylammonium bromide), showing excellent surface superhydrophobicity. By using Tafel polarization curves and electrochemical impedance spectroscopy, the corrosion protection performance of PANI with different wettability degrees was evaluated in 3.5% NaCl electrolyte. Electrochemical tests were conducted to investigate the effect of surfactant addition on the anticorrosion performance of PANI coating.

Before starting, both bare stainless steel and those coated with PANI were immersed in a corrosive medium for 30 min. Corrosion resistance was studied by plotting the polarization curves, as shown in Figure 1.6. The polarization curves for stainless steel electrodes coated with PANI showed remarkable potential shifts to positive values, and their corrosion current density decreased slightly compared to that of the uncoated electrode. The role of PANI coating is to prevent access by corrosive species into the substrate. Superhydrophobic PANI modified with the surfactant displays much better corrosion protection performance. In Figure 1.6, the PANI-PEG1 sample shows the highest corrosion potential (E_{corr}) and the lowest corrosion current density (i_{corr}), indicating the best corrosion protection performance. The corrosion potential increased with the increase of the contact angle, and better hydrophobicity corresponded to better corrosion resistance. From the foregoing, it is clear that the various superhydrophobic PANI coatings have better anticorrosion performance compared to the hydrophilic PANI.

Chromium(VI) ions with their anti-corrosion properties are often used in most anticorrosive coatings, and alternative strategies have to be tested to replace them because of their toxicity. To keep the anticorrosive property on the surface is important for practical applications in industry.

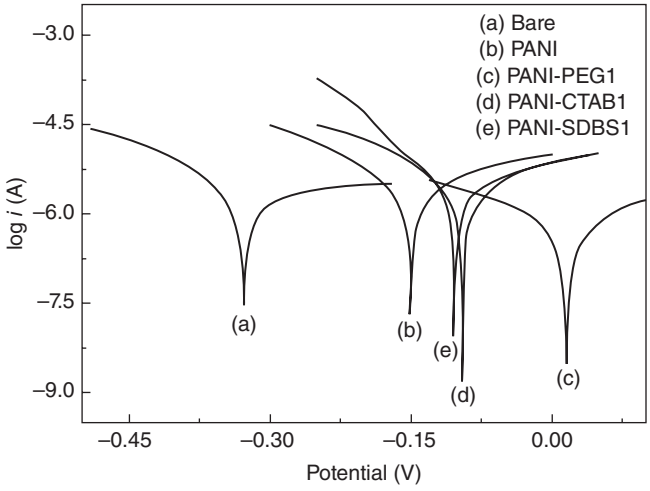

Figure 1.6 Tafel plots for bare stainless steel, stainless steel coated with PANI, PANI-PEG1, PANI-CTAB1, and PANI-SDBS1 [20].

1.4 Photochromism

It is novel and interesting to endow biomimetic superhydrophobic materials with photochromic property. After activation by a light source, photochromism refers to the reversible color transformation. And, via a facile and substrate-independent route, superhydrophobic tungsten oxide (TO) coatings with a WCA of 155° were developed by us for photochromism [21]. The preparation of superhydrophobic TO particles was based on two-step precipitation method, and the preparation of superhydrophobic coating could be achieved using a mixed resin solution. In this way, a superhydrophobic TO coating with photochromic property was prepared. After UV irradiation for 30 min, the original yellow color of the coating automatically changed to dark blue, and the intrinsic color could be fully reversed by irradiating with visible light. The reversible photochromic switch can be realized by alternating irradiation cycles.

By an inexpensive and simple electrochemical deposition process, Wang *et al.* prepared rough and photochromic TO films [22]. In their procedure, Na_2WO_4 aqueous solution was chosen as the electrolyte for the electrodeposition of TO films along with oxalic acid to adjust the solution pH in the range 3.1–8.6. Indium tin oxide (ITO) glass was used as the working electrode (with platinum as the counter-electrode and Ag/AgCl as the reference electrode), and electrochemical deposition was conducted at 1.5 eV in the single-potential time-based mode. The results indicate that the oxide films become rough with a remarkable increase of the size of the NPs upon increasing the pH value, whereas a smooth film composed of NPs is formed at low pH. When the pH of the precursor solution was ~8.6, a rough brown film was obtained that exhibited a pebble-beach-like morphology made up of many nanoprotuberances with diameters in the range 40–350 nm, as shown in Figure 1.7a,b.

TO's photochromic behavior was also studied because it is an excellent photochromic material. After UV irradiation, the as-prepared film became yellowish green from the initial brown, and when this film was placed in the dark, it recovered the brown color. As shown in Figure 1.7c, the UV spectra show a change in absorbance, with the greatest absorbance change of 0.34 occurring at ~372 nm. In addition, good reversibility was observed for many cycles of coloration and decoloration. The authors pointed out that the photochromic behavior of the as-deposited film is due to the variation of the tungsten valence as well as the number of oxygen vacancies and water molecules. Importantly, the photochromic behavior and wettability change are linked to the adsorption of atmospheric water by the film, and this work is indeed great.

The elaboration of one-dimensional nanostructures of semiconductors, such as nanorods, nanoneedles, nanowires, nanotubes, or nanobelts, can yield unique properties including photochromism. Therefore, the deposition of these nanostructures on superhydrophobic surfaces should be carried further.

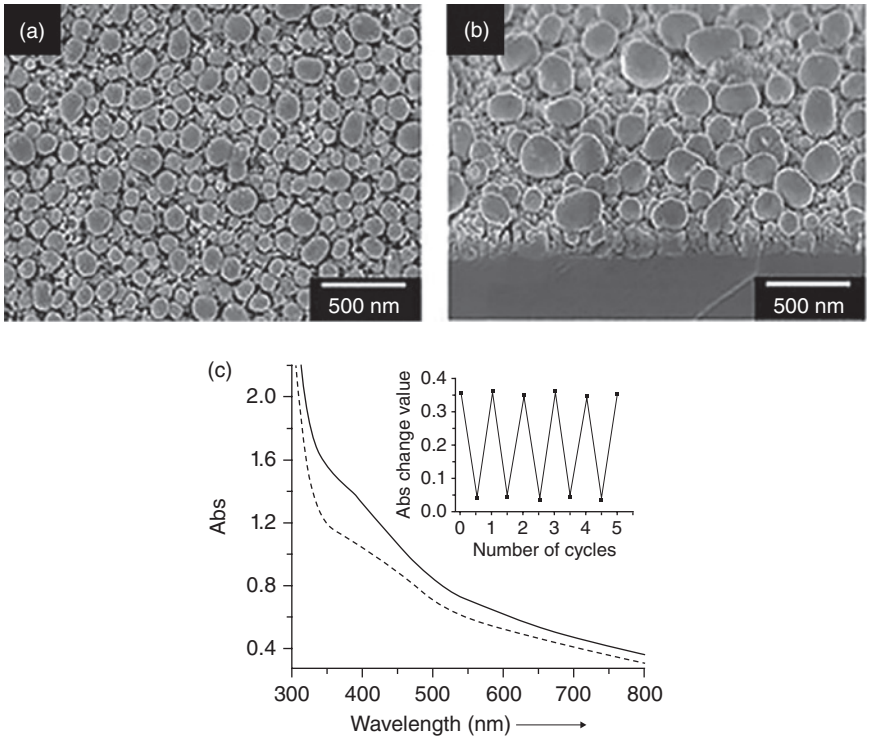

Figure 1.7 (a) Top view and (b) side view of typical SEM images of tungsten oxide films deposited from the electrolyte at a pH of ~8.6. (c) Absorption spectra of an electrodeposited tungsten oxide film before (solid line) and after (dashed line) UV light irradiation. The insert shows the photochromic switching of the absorption change (monitored at 372 nm) during consecutive cycles of UV irradiation and storage in the dark. (Wang *et al*. 2006 [22]. Reproduced with permission of John Wiley and Sons.)

1.5 Robust and Durable Superhydrophobic Materials

Many superhydrophobic surfaces have poor durability due to the fragility of the microscopic roughness features; thus, it is imperative to improve the durability of superhydrophobic surfaces for practical applications [23]. To date, a variety of durable superhydrophobic materials have been fabricated through various approaches.

With a facile one-step hydrothermal strategy, Li *et al.* coated flower-like hierarchical TiO_2 micro/NPs onto cotton fabric substrates (TiO_2@cotton) [24]. The as-prepared TiO_2@cotton exhibited good laundering durability as well as superhydrophobicity. Excellent reuse of textile fabrics is possible because of their robust laundering durability. Figure 1.8 shows the change of contact angle and adhesive force after laundering for five cycles according to the American Association of Textile Chemists and Colorists (AATCC 61-2006) standard method on superhydrophobic TiO_2@cotton fabricated at 150 °C for 20 h by a hydrothermal method. Before laundering, the superhydrophobic surface exhibited a static contact angle of ~159.0° and an adhesive force of ~12 μN. After the first laundering cycle, a slight decrease in contact angle and a notable increase (30 μN) in adhesion occurred. The surfaces still displayed superhydrophobicity after the second cycle, even in spite of the decrease of contact angle. In the next few laundering cycles, the contact angle and droplet adhesion on superhydrophobic fabric tended to remain stable. Water droplets on such superhydrophobic surface retained their spherical shape before and after laundering for five accelerated cycles, demonstrating that the superhydrophobic surface was stable. Water droplets could roll away from the surface when raised up the side of the sample. In the case of the control, the surface abruptly became highly hydrophilic combined with a high adhesion after the second laundering cycle. So decoration with the hierarchical TiO_2 particles is vital for the stability of superhydrophobicity.

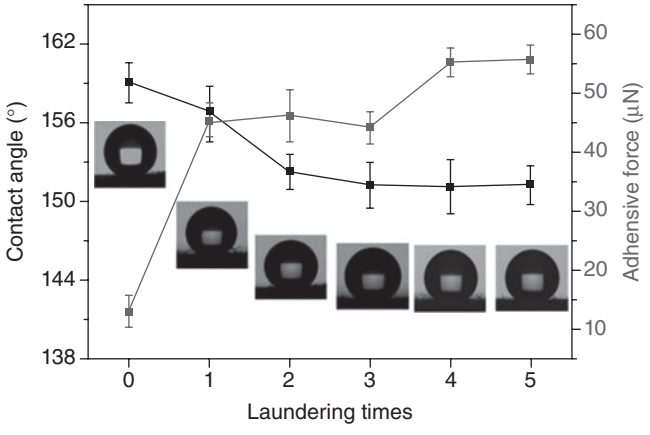

Figure 1.8 Effect of laundering cycles on the contact angle and adhesive force of TiO_2@cotton fabrics according to AATCC standard method. The insets are the corresponding contact angle images with different laundering cycles. (Li *et al.* 2015 [24]. Reproduced with permission of John Wiley and Sons.)

Robustness to flame is impossible for traditional paper, but with appropriate modification it is possible to improve this situation. As for flame retardancy, we have demonstrated one kind of omnipotent epoxy resins@stearic acid-$Mg(OH)_2$ superhydrophobic coating via a simple anti-deposition route [25]. First of all, micro- and nanosheet $Mg(OH)_2$ (MH) powder was prepared via a simple anti-deposition route. After the MH powder was modified by stearic acid (STA), the superhydrophilic MH turned into superhydrophobic STA-MH. Taking advantage of the high adhesive force of epoxy resin, epoxy resin@ STA-MH superhydrophobic coating with excellent mechanical stability could be obtained on any solid substrate. This omnipotent superhydrophobic coating not only has great water repellency but also possesses flame retardancy.

Because of the excellent flame retardancy of MH, the epoxy resin@STA-MH coating can be provided with great flame retardancy, as demonstrated by a simple vertical flame testing method. Uncoated cloth (about 2.5 cm × 4 cm), as control sample, was subjected to a flame for just 1 s and it ignited immediately. After only 20 s, the uncoated cloth burned out completely. The whole burning process took ~28 s with practically no residue, and the whole process is shown in Figure 1.9a. Under the same condition, the coated cloth sample could not be ignited completely (Figure 1.9b). So, the ignition duration was extended to 5 s for the coated sample. This time the sample was ignited. The flame still spread slowly and covered the whole sample until 30 s. The whole burning process took ~43 s, which was 1.5 times the time taken for uncoated one. By the way, the coated cloth preserved almost all residues (Figure 1.9c). At a high heat-absorbing process at 340–490 °C, the MH underwent decomposition and the heat diffusion was effectively stopped. Moreover, during this decomposition process to MgO of MH, H_2O was released, which could dilute the oxygen concentration around the flame to extinguish it. These are the two main reasons for the flame retardancy of MH. Although the flame retardancy test of the epoxy resin@STA-MH coating was carried out in the laboratory environment, and the actual effect needs to be verified in a more realistic environment, this laboratory test still could show that the epoxy resin@STA-MH coating had great flame retardancy potential. In the future, this coating can save huge loss of lives and property.

1.6 Transparent and Conductive Superhydrophobic Film

Because of the roughness factor, superhydrophobicity and transparency are generally two contradictory characteristics. Even so, much progress has been made to achieve both of these aspects. Generally, transparent superhydrophobic surfaces are mainly achieved on glass slides by dip-coating or spin-coating [26, 27]. There have been a few studies on the use of copper oxide NPs to directly fabricate an excellent superhydrophobic film with both good transparency and conductivity on various transparent substrates with the aid of PANI (an important conducting polymer). Because of its high conductivity, easy preparation, very good chemical stability, and simple non-redox acid/base doping/dedoping process, PANI has been extensively studied for potential applications including chemical sensors, actuators, anticorrosive coatings, capacitors, and nonvolatile

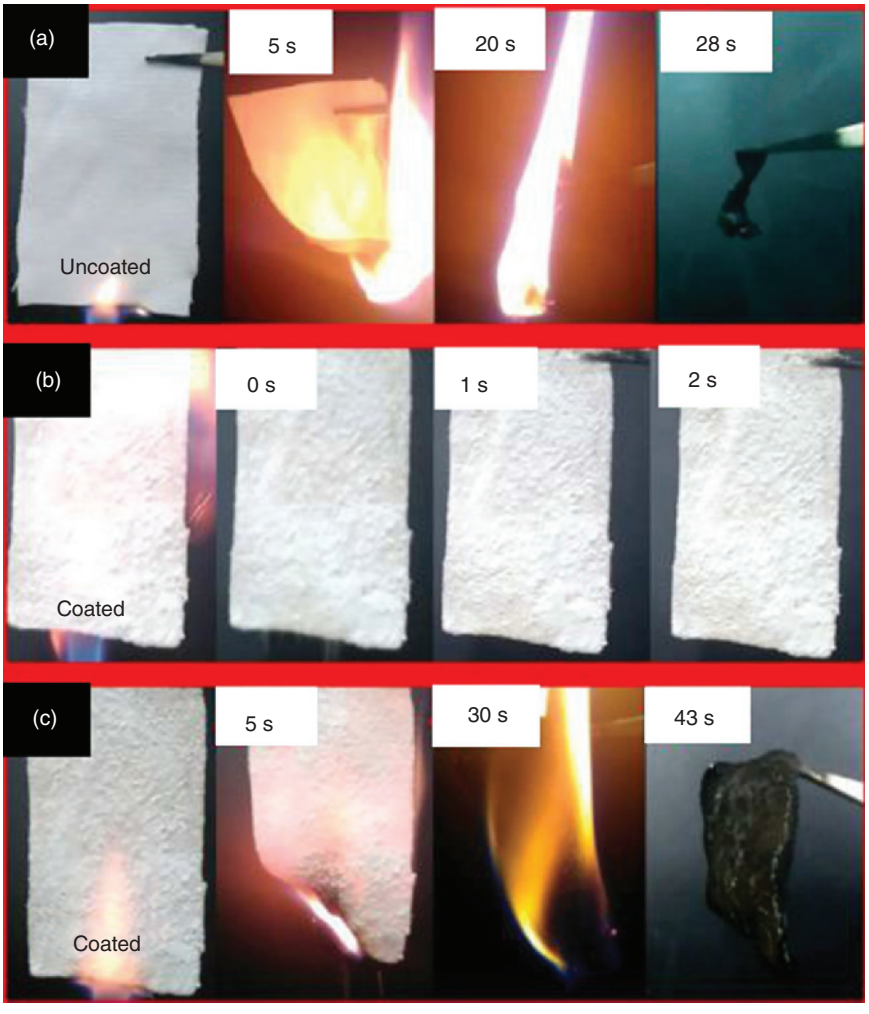

Figure 1.9 Photographs of the flame retardancy test of (a) uncoated and (b, c) coated cloth with different ignition durations (1 and 5 s, respectively). (Si *et al*. 2016 [25]. Reproduced with permission of American Chemical Society.)

plastic memory devices. PANI is usually prepared via either chemical or electrochemical polymerization. However, most studies on PANI primarily focus on its nanofibers in bulk solution. PANI nanofibers are usually formed on substrates present in the reaction system and polymerized on solid surfaces, which has drawn much interest in recent years. Our group has already fabricated transparent superhydrophobic coatings on glass with hollow SiO_2 spheres through a carbon template route [28]. Here, transparent and conductive superhydrophobic surfaces were prepared on poly(ethylene terephthalate) (PET), PS, or glass slides smoothly by an *in situ* deposition method. Before the experiment, the glass slides were immersed in hot Piranha solution for 1 h and subsequently cleaned with deionized water several times. This proved to be facile and inexpensive and of

great value in achieving high yield as well [29]. PANI nanofibers grow on various kinds of substrates, including conducting (ITO and Si wafers) and nonconducting substrates (PS, PET, glass). Various transparent substrates were used to fabricate transparent superhydrophobic surfaces by decorating them with CuO NPs over PANI nanofibers. The as-fabricated films on the substrates exhibited excellent transparency, superhydrophobicity, and conductivity.

Studies on bioinspired conductive and transparent superhydrophobic surfaces are widely reported, which are not only of interest in understanding the fundamental principles involved but also for their promising practical applications in micro- and nanomaterials and some specific devices.

1.7 Anti-fingerprint Superhydrophobic Film

Although much effort has been made to make transparent superhydrophobic surfaces recently, surfaces with robust transparent superhydrophobic plus anti-fingerprint properties have rarely been reported. The superhydrophobic surface with low energy can reduce intermolecular attractive forces. Therefore, the spreading of a contacting medium over a low-energy surface is reduced along with any physical or chemical bonds, resulting in low practical adhesion levels, which can promote the formation of anti-fingerprint coatings. For the anti-fingerprint property, the surface should have low energy, resulting in the formation of an oleophobic, weak boundary layer possibly [30]. Besides, the surface should show dissimilar solubility parameters to the contacting media to prevent interdiffusion and be thermally stable, which is essential for some applications. To this end, an industry-compatible approach was presented to make robust, transparent, and anti-fingerprint superhydrophobic surfaces [31]. The fabrication procedure starts with making a PANI nanofiber forest on stainless steel by dilute chemical polymerization. By controlling the reaction times, we were able to ensure the optimal polymerization time (10 h) to realize the best surface nanofibers. Subsequently, the superhydrophobic property was achieved by post-treatment with 1*H*,1*H*,1*H*,1*H*-perfluorodecane thiol. Thiol is a weak acid, and the modification of PANI with thiol is actually a doping process. Importantly, we particularly investigated the anti-fingerprint properties of the obtained coatings, and found that the performance could be enhanced by 80–85% compared to the bare stainless steel surface. This will open the avenue for superhydrophobic surfaces with new potential applications, such as decorative coatings on various surfaces.

1.8 Anti-icing Ability

Biomimetic superhydrophobic materials with anti-icing property have been a research area of great interest due to their significant economic, energy, and safety applications in preventing, delaying, or removing ice in many situations [32, 33]. Particularly worth mentioning is that the anti-icing properties of superhydrophobic surfaces have been verified in many great works [34, 35]. Apart from Chapter 10, here it will be briefly introduced. We have demonstrated that the

previously mentioned epoxy resin@STA-MH coating also has this anti-icing ability [25]. Both a bare glass slide and a coated glass slide were put into a refrigerator (−10 °C) with a water droplet (~40 μl) placed on each of them. The water droplet spread out on the bare glass slide but remained as spherical shape on the coated one. The changes of water droplets were recorded using a camera every 2 min. The water droplet on the bare sample took ~540 s to be converted to ice completely. However, the icing process of water droplet on coated glass slide took ~1620 s, which is 3 times as long as that of control sample. In theory, the water droplet on the surperdrophobic surface has a smaller contact area with the substrate, which provided less area for heterogeneous nucleation. On the other hand, air pockets also can obstruct the heat transfer between the water droplet and substrate, thereby extending the icing time. Furthermore, to test the anti-icing ability of the epoxy resin@STA-MH coating, a copper mesh with a higher heat transfer rate was chosen. Under the same experimental conditions, the results showed that the icing time of a water droplet on the bare copper mesh was reduced from 540 s on bare glass slide to 240 s. Likewise, the icing time of the coated copper mesh was about 480 s, which is double that of the control sample. Importantly, on tilting the copper mesh to a certain angle, in both bare and coated samples with the iced water droplet, the iced water droplet could separate itself from the coated sample while water droplet on the bare copper mesh could not do so. This phenomenon also confirmed the low adhesive force of the epoxy resin@ STA-MH coating to ice. That is to say, the superhydrophobic epoxy resin @ STA-MH coating could not only delay the icing time but also reduce the adhesive force between ice and the substrate. So, this superhydrophobic epoxy resin @ STA-MH coating can protect various coated substrates from freezing disasters in some extreme climates.

We have also reported an economical, efficient, and eco-friendly approach for the fabrication of anti-icing superhydrophobic copper materials by Fe^{3+} etching and octadecanethiol (ODT) modification [36]. The whole process takes only 10 min under ambient condition. The as-prepared copper materials not only show excellent superhydrophobicity but also prominently prolong ice over time with a long cycle life. Moreover, the facile approach can be easily scaled up for producing samples of any reasonable size. Owing to the simplicity of the method, excellent superhydrophobicity, outstanding durability, and stability, the as-prepared superhydrophobic copper surfaces are quite promising for practical applications.

For both anti-icing and de-icing functions, Yin *et al.* demonstrated the conceptual feasibility of using a self-lubricated photothermal coating [37]. The anti-icing coating is designed to be water repellent and is infiltrated with hydrocarbon or perfluorocarbon oils to endow it with a liquid interface for preventing ice accumulation or minimizing the adhesion of ice on the coated surfaces. Fe_3O_4 NPs are added to the film to afford high-efficiency photothermal effect under near-infrared irradiation for rapidly melting the accumulated ice. The authors have pointed out that this conceptual strategy can be easily implemented to fabricate analogous sprayed coatings.

In their work, different PDMS film samples were prepared for the control experiment, that is, smooth PDMS film (SF) without pores, fluorination, and lubricant; porous film (PF); fluorinated porous film (FF); and fluorinated porous film infiltrated with perfluoro polyether lubricant (LF). As shown in

Figure 1.10a–c, the ice layers formed on all films in freezing rain environment are more compact and thicker than those formed under high humidity condition. Ice balls were clearly observed on LF, whereas densely packed ice layers were formed on SF and FF. The authors explain that water droplets impacting on the rough FF surface at a certain speed tend to alter the wetting mode rapidly, while on LF the wetting property is very stable [38, 39]. The formed ice layer on films is closely related to the icing process, which has a great impact on the adhesion strength of ice on the surface [40, 41]. The ice layer adhesion strengths on three different surfaces are all much higher than that of the layer formed under humidity condition (Figure 1.10d). The ice removal must be assisted by an outside force or heat. As schematically shown in Figure 1.10e,f, Fe_3O_4 NPs are used for photoresponsive thermogenesis. The surface temperature of LF increases obviously and exceeds 50 °C after 10 s of irradiation. No obvious temperature change was detected on the undoped film even after 50 s of irradiation. Figure 1.10g shows that the ice layer melts instantaneously with the movement of the light spot. So it can be concluded that the introduction of photothermal nanomaterial obviously assists ice removal by melting the ice at the interface, which together with the lubricating property of the surface plays a synergistic role in anti-/de-icing. We believe that this great work is bound to inspire and promote the design and fabrication of anti-/de-icing materials.

In general, anti-icing research can be started from the following two aspects: delaying ice formation, and reducing ice adhesion. Because of the special interfacial wettability and adhesion of superhydrophobic surfaces and icephobic surfaces (IPSs) with water and ice, significant anti-icing performances in these two aspects have been achieved under both laboratory and natural conditions. However, the wetting, icing, and adhering behavior on the superwetting surfaces is a multifaceted interaction involving water states, surface properties, and environmental conditions. A comprehensive picture has still not been provided. In Chapter 10, we primarily investigate the ice and frost formation mechanism for the rational design of anti-icing/anti-frosting surfaces. Significantly, the complex dynamics and thermodynamics of water droplets on superhydrophobic surfaces under various freezing conditions that might be encountered in natural atmosphere are comprehensively discussed. Critically, we explain why superhydrophobic surfaces play a fairly limited role in reducing ice adhesion strength. Furthermore, a new type of superhydrophobic family of materials termed *IPSs* for effortless ice detachment is introduced. And, future challenges and possible breakthroughs in this field are pointed out. It is believed that with the unremitting efforts of scientists, second-generation anti-/de-icing materials based on superhydrophobic interfaces will be put into practical applications in the near future.

1.9 Summary

Functional biomimetic superhydrophobic materials have been widely researched in recent years, and their corresponding applications have been also developed in many fields, for example, the water-collecting materials inspired by the alternating hydrophobic and hydrophilic areas on the back surface of Namib Desert beetles

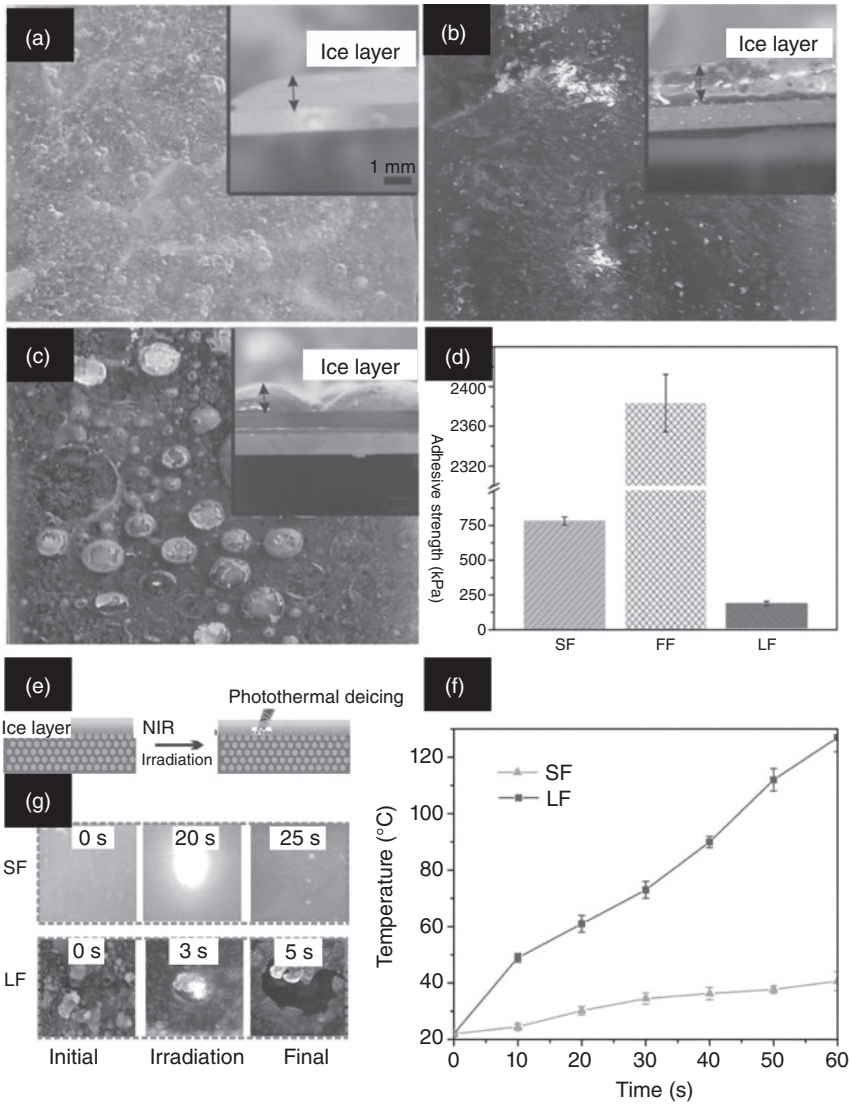

Figure 1.10 Ice formation, adhesion, and de-icing characteristics. Digital images of ice layers formed on (a) SF, (b) FF, and (c) LF under mimicked freezing rain environment. (d) Average ice adhesion strength on different films. Laser-induced photothermal deicing. (e) Schematic of the photothermal rapid de-icing process. (f) Plots of surface temperature with irradiation time at room temperature. (g) Captured images from the de-icing videos, showing the ice melting process on SF and LF at different times. Yin *et al*. 2015 [37]. Reproduced with permission of John Wiley and Sons.

and self-cleaning materials inspired by low adhesion on a lotus leaf surface. Moreover, corrosion resistance, photochromic superhydrophobicity, robust superhydrophobicity, conductive and transparent superhydrophobicity, anti-fingerprint superhydrophobicity, and the anti-icing superhydrophobicity also find applications in the fabrication of superhydrophobic materials. Although superhydrophobic

materials have been widely studied, there are still some challenges for their real applications, attributable to their chemical and mechanical instability, which calls for further and deeper understanding. Thus, to effectively broaden and improve the applications of superhydrophobic materials, much more effort is required to clarify the potential mechanism of superhydrophobicity in various natural phenomena and apply them in today's functional products for human benefit.

References

1 Snell-Rood, E. (2016) Bring biologists into biomimetics. *Nature*, **529**, 277–278.
2 Wang, S., Liu, K., Yao, X., and Jiang, L. (2015) Bioinspired surfaces with superwettability: New insight on theory, design, and applications. *Chem. Rev.*, **115**, 8230–8293.
3 Bai, F., Wu, J., Gong, G., and Guo, L. (2014) Biomimetic "water strider Leg" with highly refined nanogroove structure and remarkable water-repellent performance. *ACS Appl. Mater. Interfaces*, **6**, 16237–16242.
4 Liu, K.S. and Jiang, L. (2011) Bio-inspired design of multiscale structures for function integration. *Nano Today*, **6**, 155–175.
5 (a) Liu, K., Zhang, M., Zhai, J., Wang, J., and Jiang, L. (2008) Bioinspired construction of Mg–Li alloys surfaces with stable superhydrophobicity and improved corrosion resistance. *Appl. Phys. Lett.*, **92**, 183103; (b) Barthlott, W. and Neinhuis, C. (1997) Purity of the sacred lotus, or escape from contamination in biological surfaces. *Planta*, **202**, 1–8.
6 (a) Yao, X., Song, Y., and Jiang, L. (2011) Applications of bio-inspired special wettable surfaces. *Adv. Mater.*, **23**, 719–734; (b) Heng, X., Xiang, M., Lu, Z., and Luo, C. (2014) Branched ZnO wire structures for water collection inspired by cacti. *ACS Appl. Mater. Interfaces*, **6**, 8032–8041; (c) Hou, Y., Chen, Y., Xue, Y., Zheng, Y., and Jiang, L. (2012) Water collection behavior and hanging ability of bioinspired fiber. *Langmuir*, **28**, 4737–4743.
7 Andrew, R. and Parker, C.R.L. (2001) Water capture by a desert beetle. *Nature*, **414**, 33–34.
8 (a) Bai, H., Wang, L., Ju, J., Sun, R., Zheng, Y., and Jiang, L. (2014) Efficient water collection on integrative bioinspired surfaces with star-shaped wettability patterns. *Adv. Mater.*, **26**, 5025–5030; (b) Zheng, Y., Bai, H., Huang, Z., Tian, X., Nie, F.Q., Zhao, Y., Zhai, J., and Jiang, L. (2010) Directional water collection on wetted spider silk. *Nature*, **463**, 640–643.
9 Wang, B., Zhang, Y., Liang, W., Wang, G., Guo, Z., and Liu, W. (2014) A simple route to transform normal hydrophilic cloth into a superhydrophobic-superhydrophilic hybrid surface. *J. Mater. Chem. A*, **2**, 7845–7852.
10 Peng, Y., He, Y.X., Yang, S., Ben, S., Cao, M.Y., Li, K., Liu, K.S., and Jiang, L. (2015) Magnetically induced fog harvesting via flexible conical arrays. *Adv. Funct. Mater.*, **25**, 5967–5971.
11 Bai, H., Sun, R., Ju, J., Yao, X., Zheng, Y.M., and Jiang, L. (2011) Large-scale fabrication of bioinspired fibers for directional water collection. *Small*, **7**, 3429–3433.

12 Wang, R., Hashimoto, K., Fujishima, A., Chikuni, M., Kojima, E., Kitamura, A., Shimohigoshi, M., and Watanabe, T. (1997) Light-induced amphiphilic surfaces. *Nature*, **388**, 431–432.

13 Zhu, H. and Guo, Z. (2016) Hybrid engineered materials with high water-collecting efficiency inspired by Namib desert beetles. *Chem. Commun.*, **52**, 6809–6812.

14 Zhu, H., Yang, F., Li, J., and Guo, Z. (2016) High-efficiency water collection on biomimetic material with superwettable patterns. *Chem. Commun.*, **52** (84), 12415–12417.

15 Dong, B., Fan, D., Wang, S., and Guo, Z. (2015) An omnipotent liquid for various engineering material substrates with transparent superhydrophobicity. *Chem. Lett.*, **44**, 1245–1247.

16 Zeng, J., Wang, B., Zhang, Y., Zhu, H., and Guo, Z. (2014) Strong amphiphobic porous films with oily-self-cleaning property beyond nature. *Chem. Lett.*, **43**, 1566–1568.

17 Wang, H. and Guo, Z. (2014) Design of underwater superoleophobic TiO_2 coatings with additional photo-induced self-cleaning properties by one-step route bio-inspired from fish scales. *Appl. Phys. Lett.*, **104**, 183703.

18 Yu, S. and Guo, Z. (2015) Superhydrophobic surfaces based on polypyrrole with corrosion resistance and the separation of oil/water mixtures properties. *RSC Adv.*, **5**, 107880–107888.

19 Feng, L., Yan, Z., Qiang, X., Wang, Y., and Liu, Y. (2015) Polystyrene-grafted Al surface with excellent superhydrophobicity and corrosion resistance. *Surf. Interface Anal.*, **47**, 506–513.

20 Xu, H., Chen, Y., Tang, J., and Zhao, Z. (2016) Facile fabrication of superhydrophobic polyaniline structures and their anticorrosive properties. *J. Appl. Polym. Sci.*, **133**, 44248–44255.

21 Jiang, T. and Guo, Z. (2016) Robust superhydrophobic tungsten oxide coatings with photochromism and UV durability properties. *Appl. Surf. Sci.*, **387**, 412–418.

22 Wang, S., Feng, X., Yao, J., and Jiang, L. (2006) Controlling wettability and photochromism in a dual-responsive tungsten oxide film. *Angew. Chem. Int. Ed.*, **118**, 1286–1289.

23 Chen, K., Wu, Y., Zhou, S., and Wu, L. (2016) Recent development of durable and self-healing surfaces with special wettability. *Macromol. Rapid Commun.*, **37**, 463–485.

24 Li, S., Huang, J., Ge, M., Cao, C., Deng, S., Zhang, S., Chen, G., Zhang, K., Al-Deyab, S.S., and Lai, Y. (2015) Robust flower-like TiO_2@cotton fabrics with special wettability for effective self-cleaning and versatile oil/water separation. *Adv. Mater. Interfaces*, **2**, 1500220.

25 Si, Y., Guo, Z., and Liu, W. (2016) A robust epoxy resins @ stearic acid-$Mg(OH)_2$ micro-nanosheet superhydrophobic omnipotent protective coating for real life applications. *ACS Appl. Mater. Interfaces*, **8**, 16511–16520.

26 Ling, X.Y., Phang, I.Y., Vancso, G.J., Huskens, J., and Reinhoudt, D.N. (2009) Stable and transparent superhydrophobic nanoparticle films. *Langmuir*, **25**, 3260–3263.

27 Xu, Q.F., Wang, J.N., Smith, I.H., and Sanderson, K.D. (2009) Superhydrophobic and transparent coatings based on removable polymeric spheres. *J. Mater. Chem.*, **19**, 655–660.

28 Chen, Y., Zhang, Y., Shi, L., Li, J., Xin, Y., Yang, T., and Guo, Z. (2012) Transparent superhydrophobic/superhydrophilic coatings for self-cleaning and anti-fogging. *Appl. Phys. Lett.*, **101**, 033701.

29 Wang, G., Liang, W., Wang, B., Zhang, Y., Li, J., Shi, L., and Guo, Z. (2013) Conductive and transparent superhydrophobic films on various substrates by in situ deposition. *Appl. Phys. Lett.*, **102**, 203703.

30 Wu, L.Y.L., Ngian, S.K., Chen, Z., and Xuan, D.T.T. (2011) Quantitative test method for evaluation of anti-fingerprint property of coated surfaces. *Appl. Surf. Sci.*, **257**, 2965–2969.

31 Wang, G., Wang, H., and Guo, Z. (2013) A robust transparent and anti-fingerprint superhydrophobic film. *Chem. Commun.*, **49**, 7310–7312.

32 Lv, J.Y., Song, Y.L., Jiang, L., and Wang, J.J. (2014) Bio-inspired strategies for anti-icing. *ACS Nano*, **8**, 3152–3169.

33 Lee, H.J. (2012) Design and development of anti-icing textile surfaces. *J. Mater. Sci.*, **47**, 5114–5120.

34 Zhao, Y., Luo, Y., Zhu, J., Li, J., and Gao, X. (2015) Copper-based ultrathin nickel nanocone films with high-efficiency dropwise condensation heat transfer performance. *ACS Appl. Mater. Interfaces*, **7**, 11719–11723.

35 Kim, A., Lee, C., Kim, H., and Kim, J. (2015) Simple approach to superhydrophobic nanostructured Al for practical antifrosting application based on enhanced self-propelled jumping droplets. *ACS Appl. Mater. Interfaces*, **7**, 7206–7213.

36 Guo, J., Yang, F., and Guo, Z. (2015) Fabrication of stable and durable superhydrophobic surface on copper substrates for oil-water separation and ice-over delay. *J. Colloid Interface Sci.*, **466**, 36–43.

37 Yin, X., Zhang, Y., Wang, D., Liu, Z., Liu, Y., Pei, X., Yu, B., and Zhou, F. (2015) Integration of self-lubrication and near-infrared photothermogenesis for excellent anti-icing/deicing performance. *Adv. Funct. Mater.*, **25**, 4237–4245.

38 Nosonovsky, M. and Hejazi, V. (2012) Why superhydrophobic surfaces are not always icephobic. *ACS Nano*, **6**, 8488–8491.

39 Bird, J.C., Dhiman, R., Kwon, H.M., and Varanasi, K.K. (2013) Reducing the contact time of a bouncing drop. *Nature*, **503**, 385–388.

40 Varanasi, K.K., Deng, T., Smith, J.D., Hsu, M., and Bhate, N. (2010) Frost formation and ice adhesion on superhydrophobic surfaces. *Appl. Phys. Lett.*, **97** (23), 234102.

41 Zhu, C.H., Lu, Y., Chen, J.F., and Yu, S.H. (2014) Photothermal poly(N-isopropylacrylamide)/Fe_3O_4 nanocomposite hydrogel as a movable position heating source under remote control. *Small*, **10**, 2796–2800.